

# Orthogonally polarized dual-wavelength Nd:LuVO<sub>4</sub> laser at 1086 nm and 1089 nm

Y. P. Huang, C. Y. Cho, Y. J. Huang, and Y. F. Chen\*

Department of Electrophysics, National Chiao Tung University, 1001 TA Hsueh Road, Hsinchu, Taiwan  
\*yfchen@cc.nctu.edu.tw

**Abstract:** A comparison between the fluorescence spectra of the Nd-doped vanadate crystals (Nd:YVO<sub>4</sub>, Nd:GdVO<sub>4</sub>, Nd:LuVO<sub>4</sub>) for the  ${}^4F_{3/2} \rightarrow {}^4I_{11/2}$  transition is studied. We numerically analyze the condition of gain-to-loss balance via an uncoated intracavity etalon to achieve the dual-wavelength operation. We further experimentally demonstrate the orthogonally polarized dual-wavelength laser with a single Nd:LuVO<sub>4</sub> crystal. The simultaneous dual-wavelength Nd:LuVO<sub>4</sub> laser at 1085.7 nm in  $\sigma$  polarization and 1088.5 nm in  $\pi$  polarization is realized. At an incident pump power of 12 W, the average output power obtained at 1085.7 nm and 1088.5 nm is 0.4 W and 1.7 W, respectively.

©2012 Optical Society of America

OCIS codes: (140.3410) Laser resonators; (140.3580) Lasers, solid-state.

---

## References and links

1. F. Weigl, "A generalized technique of two-wavelength, nondiffuse holographic interferometry," *Appl. Opt.* **10**(1), 187–192 (1971).
2. N. G. Basov, M. A. Gubin, V. V. Nikitin, A. V. Nikuchin, V. N. Petrovskii, E. D. Protsenko, and D. A. Tyurikov, "Highly-sensitive method of narrow spectral-line separations, based on the detection of frequency resonances of a 2-mode gas-laser with non-linear absorption," *Izv. Akad. Nauk SSSR, Ser. Fiz.* **46**, 1573–1583 (1982).
3. R. W. Farley and P. D. Dao, "Development of an intracavity-summed multiple-wavelength Nd:YAG laser for a rugged, solid-state sodium lidar system," *Appl. Opt.* **34**(21), 4269–4273 (1995).
4. Y. F. Chen, Y. S. Chen, and S. W. Tsai, "Diode-pumped Q-switched laser with intracavity sum frequency mixing in periodically poled KTP," *Appl. Phys. B* **79**(2), 207–210 (2004).
5. S. N. Son, J. J. Song, J. U. Kang, and C. S. Kim, "Simultaneous second harmonic generation of multiple wavelength laser outputs for medical sensing," *Sensors (Basel)* **11**(6), 6125–6130 (2011).
6. Y. Lu, B. G. Zhang, E. B. Li, D. G. Xu, R. Zhou, X. Zhao, F. Ji, T. L. Zhang, P. Wang, and J. Q. Yao, "High-power simultaneous dual-wavelength emission of an end-pumped Nd:YAG laser using the quasi-three-level and the four-level transition," *Opt. Commun.* **262**(2), 241–245 (2006).
7. K. Lünstedt, N. Pavel, K. Petermann, and G. Huber, "Continuous-wave simultaneous dual-wavelength operation at 912 and 1063 nm in Nd:GdVO<sub>4</sub>," *Appl. Phys. B* **86**(1), 65–70 (2007).
8. H. Y. Shen, R. R. Zeng, Y. P. Zhou, G. F. Yu, C. H. Huang, Z. D. Zeng, W. J. Zhang, and Q. J. Ye, "Simultaneous multiple wavelength laser action in various Neodymium host crystals," *IEEE J. Quantum Electron.* **27**(10), 2315–2318 (1991).
9. Y. F. Chen, "CW dual-wavelength operation of a diode-end-pumped Nd:YVO<sub>4</sub> laser," *Appl. Phys. B* **70**(4), 475–478 (2000).
10. X. Yu, C. L. Li, G. C. Sun, B. Z. Li, X. Y. Chen, M. Zhao, J. B. Wang, X. H. Zhang, and G. Y. Jin, "Continuous-wave dual-wavelength operation of a diode-end-pumped Nd:LuVO<sub>4</sub> laser," *Laser Phys.* **21**(6), 1039–1041 (2011).
11. H. H. Yu, H. J. Zhang, Z. P. Wang, J. Y. Wang, Y. G. Yu, Z. B. Shi, X. Y. Zhang, and M. H. Jiang, "High-power dual-wavelength laser with disordered Nd:CNGG crystals," *Opt. Lett.* **34**(2), 151–153 (2009).
12. H. H. Yu, H. J. Zhang, Z. P. Wang, J. Y. Wang, Y. G. Yu, X. Y. Zhang, R. J. Lan, and M. H. Jiang, "Dual-wavelength neodymium-doped yttrium aluminum garnet laser with chromium-doped yttrium aluminum garnet as frequency selector," *Appl. Phys. Lett.* **94**(4), 041126 (2009).
13. R. Zhou, B. G. Zhang, X. Ding, Z. Q. Cai, W. Q. Wen, P. Wang, and J. Q. Yao, "Continuous-wave operation at 1386 nm in a diode-end-pumped Nd:YVO<sub>4</sub> laser," *Opt. Express* **13**(15), 5818–5824 (2005).
14. H. Y. Zhu, G. Zhang, C. H. Huang, Y. Wei, L. X. Huang, A. H. Li, and Z. Q. Chen, "1318.8 nm/1338.2 nm simultaneous dual-wavelength Q-switched Nd:YAG laser," *Appl. Phys. B* **90**(3-4), 451–454 (2008).
15. Y. F. Chen, M. L. Ku, and K. W. Su, "High-power efficient tunable Nd:GdVO<sub>4</sub> laser at 1083 nm," *Opt. Lett.* **30**(16), 2107–2109 (2005).
16. W. Shi, Y. J. Ding, N. Ferneliuss, and K. Vodopyanov, "Efficient, tunable, and coherent 0.18–5.27-THz source based on GaSe crystal," *Opt. Lett.* **27**(16), 1454–1456 (2002).

17. J. F. Federici, B. Schulkin, F. Huang, D. Gary, R. Barat, F. Oliveira, and D. Zimdars, "THz imaging and sensing for security applications—explosives, weapons and drugs," *Semicond. Sci. Technol.* **20**(7), S266–S280 (2005).
18. J. B. Baxter and G. W. Guglietta, "Terahertz spectroscopy," *Anal. Chem.* **83**(12), 4342–4368 (2011).
19. C. B. Reid, E. Pickwell-MacPherson, J. G. Lauffer, A. P. Gibson, J. C. Hebden, and V. P. Wallace, "Accuracy and resolution of THz reflection spectroscopy for medical imaging," *Phys. Med. Biol.* **55**(16), 4825–4838 (2010).
20. L. G. Fei and S. L. Zhang, "The discovery of nanometer fringes in laser self-mixing interference," *Opt. Commun.* **273**(1), 226–230 (2007).
21. S. L. Zhang, Y. D. Tan, and Y. Li, "Orthogonally polarized dual frequency lasers and applications in self-sensing metrology," *Meas. Sci. Technol.* **21**(5), 054016 (2010).
22. C. Ren and S. L. Zhang, "Diode-pumped dual-frequency microchip Nd:YAG laser with tunable frequency difference," *J. Phys. D Appl. Phys.* **42**(15), 155107 (2009).
23. X. P. Yan, Q. Liu, H. L. Chen, F. Xing, M. L. Gong, and D. S. Wang, "A novel orthogonally linearly polarized Nd:YVO<sub>4</sub> laser," *Chin. Phys. B* **19**(8), 084202 (2010).
24. B. Wu, P. P. Jiang, D. Z. Yang, T. Chen, J. Kong, and Y. H. Shen, "Compact dual-wavelength Nd:GdVO<sub>4</sub> laser working at 1063 and 1065 nm," *Opt. Express* **17**(8), 6004–6009 (2009).
25. C. Maunier, J. L. Doualan, R. Moncorge, A. Speghini, M. Bettinelli, and E. Cavalli, "Growth, spectroscopic characterization, and laser performance of Nd:LuVO<sub>4</sub>, a new infrared laser material that is suitable for diode pumping," *J. Opt. Soc. Am. B* **19**(8), 1794–1800 (2002).
26. Y. F. Chen, "cw dual-wavelength operation of a diode-pumped Nd:YVO<sub>4</sub> laser," *Appl. Phys. B* **70**(4), 475–478 (2000).
27. C. A. Bennett, *Principles of Physical Optics* (Wiley, 2008).

## 1. Introduction

Simultaneous dual-wavelength laser has been of great interest for many applications such as medical instrumentation, precision laser spectroscopy, holography, lidar, and scientific research of nonlinear optical mixers [1–5]. Rare-earth-doped laser media possessing many sharp fluorescent lines, especially in the  ${}^4F_{3/2} \rightarrow {}^4I_{11/2}$  transition, are natural candidates to realize the simultaneous dual-wavelength solid-state lasers. Neodymium (Nd) lasers, because of their high gains and the good thermal and mechanical properties, are by far the most important solid-state lasers. The realized simultaneous dual-wavelength lasers in Nd host crystals can be classified into three main types. The first type involving two different laser transitions from  ${}^4F_{3/2} \rightarrow {}^4I_{11/2}$ ,  ${}^4F_{3/2} \rightarrow {}^4I_{13/2}$ , or  ${}^4F_{3/2} \rightarrow {}^4I_{9/2}$  gives a large wavelength separation with a single polarization [6–10]. The second type is the laser operated in the same laser transition with a smaller wavelength separation and a single polarization [11–15], which is very attractive for coherent terahertz (THz) generation by nonlinear difference frequency mixing [16]. Coherent THz waves, traditionally defined in the frequency range of 0.1–3 THz, have great potential for THz imaging, sensing and THz spectroscopy applications [17–19]. The dual-wavelength lasers with orthogonal polarizations, classifying as the third type, are desirable for the applications of laser interferometry and precision metrology [20,21]. Nd:YAG, Nd:YVO<sub>4</sub>, and Nd:GdVO<sub>4</sub> lasers have been demonstrated recently to achieve the simultaneous emissions of two orthogonally polarized wavelengths, in which an additional birefringent element or second gain medium was employed for obtaining orthogonal linear polarizations [22–24]. It will be more practically desirable and convenient to develop a compact orthogonally polarized dual-wavelength laser with a single gain medium in a simple cavity.

In this work, we first make a comparison between the fluorescence spectra of Nd:YVO<sub>4</sub>, Nd:GdVO<sub>4</sub> and Nd:LuVO<sub>4</sub> crystals for the  ${}^4F_{3/2} \rightarrow {}^4I_{11/2}$  transition. It is found that the spontaneous emission spectra of Nd:LuVO<sub>4</sub> crystals in the range of 1080 nm and 1090 nm display comparable radiation strengths in  $\pi$  and  $\sigma$  polarizations. Comparing to the properties of Nd:YVO<sub>4</sub> and Nd:GdVO<sub>4</sub> crystals, the Nd:LuVO<sub>4</sub> crystal possesses a wider separation between the fluorescence peak positions of  $\pi$  and  $\sigma$  polarizations near 1080–1090 nm. With these superior properties, we numerically analyze the condition of gain-to-loss balance via an uncoated intracavity etalon to achieve the dual-wavelength operation in a Nd:LuVO<sub>4</sub> laser. Finally, we experimentally accomplish a diode-end-pumped dual-wavelength Nd:LuVO<sub>4</sub> laser with orthogonal  $\sigma$  and  $\pi$  polarizations at 1085.7 nm and 1088.5 nm, respectively. At an incident pump power of 12 W, the output powers of 0.4 W at 1085.7 nm and of 1.7 W and 1088.5 nm are simultaneously obtained.

## 2. Fluorescence spectra of Nd:YVO<sub>4</sub>, Nd:GdVO<sub>4</sub> and Nd:LuVO<sub>4</sub> crystals

Vanadate family crystals doped with Nd<sup>3+</sup> ions, such as Nd:YVO<sub>4</sub>, Nd:GdVO<sub>4</sub> and Nd:LuVO<sub>4</sub>, have been recognized as the excellent active media for diode-pumped solid-state lasers due to their broad absorption bands, large absorption and emission cross sections. Nd-doped vanadate crystals, however, are characterized by their polarization-dependent gains. We experimentally study the fluorescence properties of Nd:YVO<sub>4</sub>, Nd:GdVO<sub>4</sub> and Nd:LuVO<sub>4</sub> crystals with doping concentrations of 0.25%, 0.5%, and 0.5%, respectively. Three crystals were cut along the *a* axis with dimensions of 3 × 3 × 8 mm<sup>3</sup> in size. Both end faces of the crystals were antireflection coated at 808 nm for diode pumping. Figure 1 displays the room-temperature polarized fluorescence spectra of the Nd:YVO<sub>4</sub>, Nd:GdVO<sub>4</sub> and Nd:LuVO<sub>4</sub> crystals for the <sup>4</sup>F<sub>3/2</sub> → <sup>4</sup>I<sub>11/2</sub> laser transition which are relative emission-line intensities measurements for the respective crystals. The spectral information was monitored by an optical spectrum analyzer (Advantest Q8381A) that employs a diffraction grating monochromator with the resolution of 0.1 nm. The blue and red curves represent the π and σ polarizations, respectively. As shown in Fig. 1(a), the strongest emission lines of three laser materials are typically near 1060 nm in π polarization, about several times higher than that in σ polarization. Unfortunately, it is considerably difficult to realize an orthogonal-polarization dual-wavelength laser with a single laser crystal near 1060 nm due to the extremely intense gain competition between two polarizations. It is obviously seen that all three crystals exhibit the significant secondary emission lines in the range of 1080–1090 nm with comparable emission intensity in π and σ polarizations. However, the spectral characteristics are extremely different in the three crystals, as shown in Fig. 1(b). The spectrum of Nd:GdVO<sub>4</sub> crystal reveals a large overlap between the emission distributions in π and σ polarizations. On the other hand, the separation between the fluorescence peak positions of π and σ polarizations in the Nd:LuVO<sub>4</sub> crystal is considerably wider than that in the Nd:YVO<sub>4</sub> crystal. As a consequence, the Nd:LuVO<sub>4</sub> crystal is superior to the Nd:YVO<sub>4</sub> and Nd:GdVO<sub>4</sub> media for achieving an orthogonally polarized dual-wavelength laser near 1080–1090 nm, which can be used as a light source to generate the THz-frequency radiation.

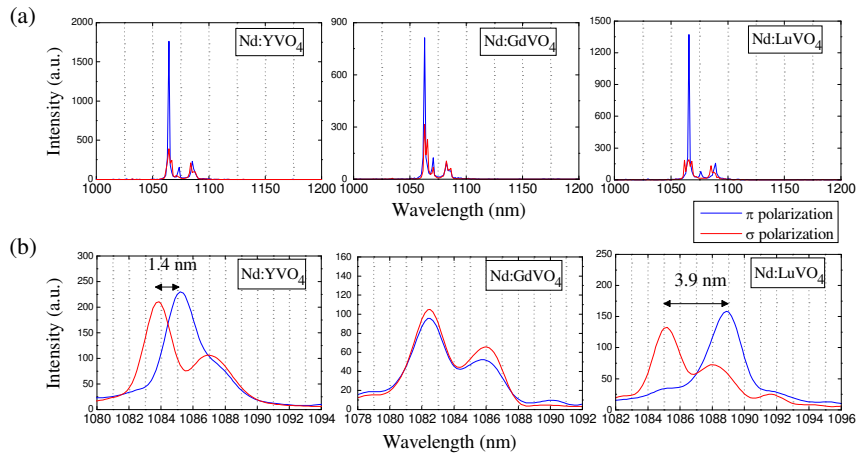


Fig. 1. (a) Fluorescence emission spectra for the <sup>4</sup>F<sub>3/2</sub> → <sup>4</sup>I<sub>11/2</sub> laser transition in the Nd:YVO<sub>4</sub>, Nd:GdVO<sub>4</sub> and Nd:LuVO<sub>4</sub> crystals at room temperature; (b) fragments of the room-temperature fluorescence spectra near 1080 and 1090 nm.

## 3. Numerical analysis for dual-wavelength operation

We analyze the dual-wavelength operation with the Nd:LuVO<sub>4</sub> crystal in the range of 1080–1090 nm under the circumstance of suppressing the strongest emission line near 1060 nm. As shown in the fluorescence spectrum, the Nd:LuVO<sub>4</sub> crystal has the comparable emission cross sections in σ and π polarizations that are respectively near 1086 nm ( $\sim 18 \times 10^{-20}$  cm<sup>2</sup>) and

1089 nm ( $\sim 20 \times 10^{-20} \text{ cm}^2$ ) [25]. The threshold condition for each transition wavelength in a simultaneous dual-wavelength operation is given by [26]

$$P_{th,i} = \frac{\ln(1/R_i) + L_i}{2l\eta_i} \frac{h\nu_p}{\sigma_i \tau_i} \frac{1}{\iiint s_i(r,z)r_p(r,z)dV}, \quad i=1,2, \quad (1)$$

where  $R_i$ ,  $L_i$ ,  $\eta_i$ ,  $\sigma_i$ , and  $\tau_i$  are, respectively, the reflectivity, the cavity round-trip loss, the quantum efficiency, the stimulated emission cross section, and the fluorescence lifetime at the upper level for the corresponding transition wavelength. Parameters of  $h\nu_p$ ,  $l$ ,  $s_i(r,z)$ , and  $r_p(r,z)$  are the pump photon energy, the length of gain medium, the normalized cavity mode intensity distribution for the corresponding transition wavelength, and the normalized pump intensity distribution in the laser cavity. Here  $i = 1, 2$  represents the two wavelengths of 1086 nm and 1089 nm, respectively. Since the two nearly close wavelengths transmitting from the same upper and lower level in the same cavity, the parameters of  $\eta_i$ ,  $\tau_i$ ,  $s_i(r,z)$ , and  $r_p(r,z)$  can be reasonably considered to be equal. Therefore, the ratio of laser thresholds for 1089 nm and 1086 nm can be expressed as:

$$\gamma = \frac{P_{th,2}}{P_{th,1}} = \frac{\ln(1/R_2) + L_2}{\ln(1/R_1) + L_1} \frac{\sigma_1}{\sigma_2}. \quad (2)$$

Since  $\sigma_1 < \sigma_2$  and the values of the reflectivity at 1086 nm and 1089 nm are usually nearly equal, i.e.  $R_1 \cong R_2$ , the ratio  $\gamma$  is less than one without introducing the deliberate difference for losses  $L_1$  and  $L_2$ . The result of  $\gamma < 1$  indicates that the laser will be dominated at 1089 nm because this emission line has a lower threshold and a higher stimulated cross section. For obtaining a dual-wavelength operation, an appropriate difference for losses  $L_1$  and  $L_2$  needs to be introduced to reach the condition of  $\gamma > 1$ . The result of  $\gamma > 1$  means that the laser will first emit the radiation at the weaker line at 1086 nm and then simultaneously emit the radiation at 1089 nm under a higher pump power.

Next we numerically verify that a uncoated intracavity etalon can be utilized to adjust the difference for losses  $L_1$  and  $L_2$  based on the dependence of Fresnel reflection upon the incident angle as well as the electric field polarization. The  $c$  axis of Nd:LuVO<sub>4</sub> crystal is set to be placed in the vertical direction, and the angle of inclination of the etalon is relative to the optical axis of the resonator, which the plane of incidence is in the horizontal direction. As a result, the  $\pi$  and  $\sigma$  polarized waves are perpendicularly and parallel to the plane of incidence, corresponding to the  $S$  and  $P$  waves respectively. The inclined angle of the etalon is equal to the incident angle of light. In terms of incident angle  $\theta$ , the losses caused by the Fresnel reflection for  $S$  and  $P$  waves can be given by [27]

$$L_S = R_S(n, \theta) + [1 - R_S(n, \theta)] \cdot R_S(1/n, \sin^{-1}(\sin \theta / n)) \quad (3)$$

and

$$L_P = R_P(n, \theta) + [1 - R_P(n, \theta)] \cdot R_P(1/n, \sin^{-1}(\sin \theta / n)), \quad (4)$$

where

$$R_S(n, \theta) = \left| \frac{\cos \theta - \sqrt{n^2 - \sin^2 \theta}}{\cos \theta + \sqrt{n^2 - \sin^2 \theta}} \right|^2, \quad R_P(n, \theta) = \left| \frac{\sqrt{n^2 - \sin^2 \theta} - n^2 \cos \theta}{\sqrt{n^2 - \sin^2 \theta} + n^2 \cos \theta} \right|^2, \quad (5)$$

and  $n$  is the ratio of the refractive indices for the etalon and air. With Eqs. (2)-(5) and the parameters in the experiment:  $\sigma_1 = 18 \times 10^{-20} \text{ cm}^2$ ,  $\sigma_2 = 20 \times 10^{-20} \text{ cm}^2$ ,  $n = 1.5$ ,  $R_1 = R_2 = 0.92$ , the losses for  $S$  and  $P$  waves and the ratio of laser thresholds  $\gamma$  are calculated as a function of incident angle  $\theta$ . It can be seen in Fig. 2(a) that the overlapping curves for the losses  $L_S$  and  $L_P$  at the small incident angle, and then gradually separate. As shown in Fig.

2(b), the ratio of laser thresholds  $\gamma$  increases with the incident angle, reaches a maximum, and then falls with further increase in the incident angle. In experiment, we will control the incident angle  $\theta$  to be approximately 30 degrees to obtain a ratio of  $\gamma = 1.5$  for achieving a dual-wavelength operation.

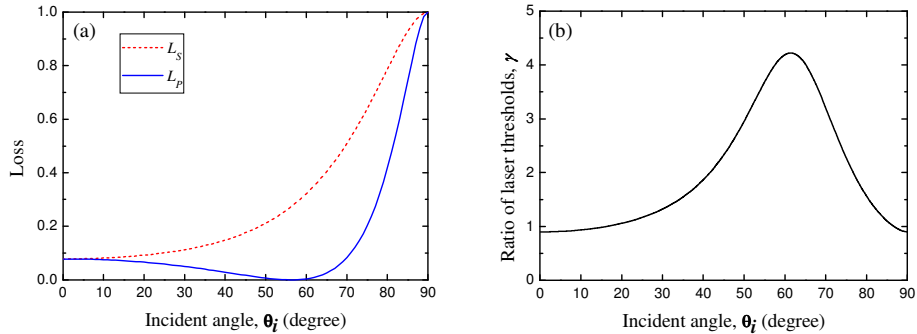


Fig. 2. Calculated results for the dependence of (a) the losses for S and P waves and (b) the ratio of laser thresholds on the incident angle for dual-wavelength operation.

#### 4. Experimental results and discussions

A sketch of the experimental scheme for a cw simultaneous dual-wavelength generation with orthogonal polarizations is presented in Fig. 3. The gain medium was 0.5 at. % Nd:LuVO<sub>4</sub> crystal with a length of 8 mm cut along the *a* axis. Both facets of the laser crystal were antireflection-coated at 808 nm and 1080–1100 nm ( $R < 0.2\%$ ). The pump source was a 12-W 808-nm fiber-coupled laser diode with a 600- $\mu\text{m}$  fiber core diameter and a numerical aperture of 0.16, reimaged into the laser crystal through a pair of focusing lenses with a focal length of 5 mm and 90% coupling efficiency. The pump spot radius was approximately 200  $\mu\text{m}$ . The input mirror was a 100-cm radius-of-curvature concave mirror with antireflection coating at 808 nm ( $R < 0.2\%$ ) on the entrance face and with high-reflectance coating at 1000–1100 nm ( $R > 99.8\%$ ) and high-transmittance coating at 808 nm ( $T > 85\%$ ) on the second surface. The output coupler was a flat mirror with transmission of 7% near 1090 nm and high transmission at 1064 nm ( $T > 85\%$ ) for suppressing the gain oscillation at 1064 nm. The measured transmittance curve for the output coupler is inserted in Fig. 3. An uncoated glass etalon with a thickness of 0.155 mm was used to nearly fit the wavelength separation between two fluorescence peak positions of  $\pi$  and  $\sigma$  polarizations near 1080–1090 nm in Nd:LuVO<sub>4</sub> crystal. The laser crystal was wrapped with indium foil and mounted in a water-cooled copper heat sink at 20°C. The cavity length was approximately 17 mm.

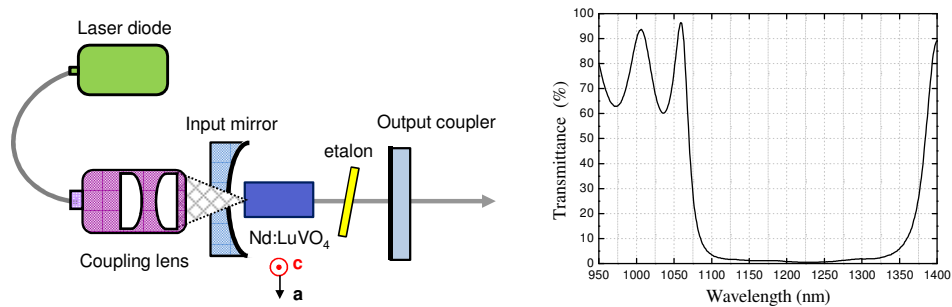


Fig. 3. Schematic of the experimental setup for the dual-wavelength Nd:LuVO<sub>4</sub> laser. Right: Measured transmittance curve for the output coupler.

First of all, the cw laser operation without an etalon was performed to study the Nd:LuVO<sub>4</sub> laser characteristics. Figure 4 presents the dependence of the average output power on the incident pump power for the single-wavelength Nd:LuVO<sub>4</sub> laser at 1089.5 nm. The pump threshold is 0.63 W. The average output power reaches 3.6 W at 12 W of incident pump power. The corresponding optical-to-optical conversion efficiency is 30% with a slope efficiency of approximately 35%. The measured optical spectrum at the maximum output power is depicted in the inset of Fig. 4. The spectral linewidth (FWHM) is about 0.4 nm with the central wavelength at 1089.5 nm. Note that the present laser output is linearly polarized along the  $\pi$  direction.

For achieving the dual-wavelength operation, an uncoated glass etalon was inserted in the laser cavity. By adjusting the inclination of the etalon relative to the optical axis of the resonator, we realized the simultaneous dual-wavelength lasing regime. At an inclined angle near 30 degrees, the dual-wavelength emission at 1086 nm and 1089 nm with orthogonal polarizations was achieved. The dual-wavelength laser was separated into two orthogonally polarized beams with a polarizing beam splitter (PBS), and the average output power for individual wavelengths were measured simultaneously. Figure 5 shows the average output power at each lasing wavelength with respect to the incident pump power at 808 nm. It can be found that the 1086 nm ( $\sigma$  polarization) is lasing prior to the 1089 nm ( $\pi$  polarization) light due to the initial suppression of  $\pi$  polarization by the inclined etalon. The threshold pump power is 4.1 W for 1086 nm, and 5.7 W for 1089 nm, which accords with the calculated result in Fig. 2(b). The output power of 1086-nm line first increases linearly with the pump power, reaches its maximum power of 0.84 W at the pump power of 7.5 W, and then rises monotonically. On the other hand, the output power of 1089-nm line increases linearly as the pump power increases, reaches the intersection of the 1089-nm and 1086-nm curves with an equal power of 0.73 W at the pump power of 8.8 W, and then generates 1.7 W at 12 W of pump power. We believe that the gain competition between 1086-nm and 1089-nm lines leads to the output power of 1086 nm decreases over 7.5 W of pump power. The cw laser operation has good temporal stability without power competition between the two wavelengths. It is worthwhile to mention that the equal power operation of 1086-nm and 1089-nm lines at higher pump power can be promoted by re-angling the etalon.

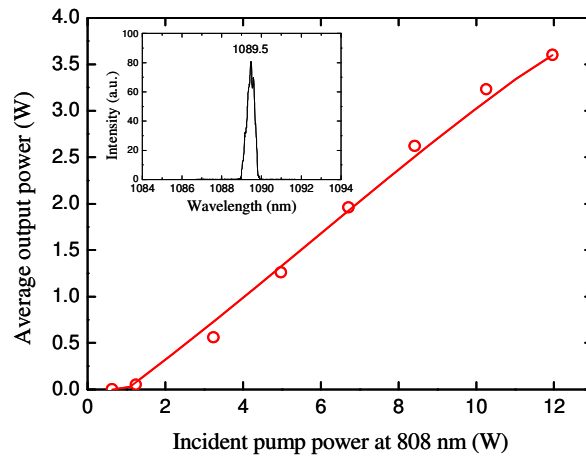


Fig. 4. Average output power versus the incident pump power for single-wavelength operation. Inset, optical spectrum of single-wavelength operation at the maximum output power.

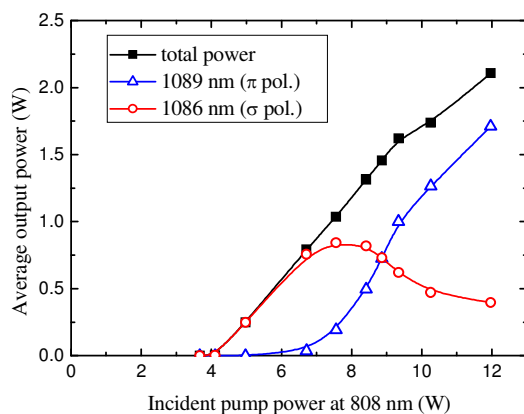


Fig. 5. Average output powers versus the incident pump power for dual-wavelength operation.

The laser beams of both the two polarizations were observed at different pump powers. The  $M^2$  factor of  $\sigma$  polarization is estimated to be approximately 1.1 near threshold, and then increases to be 2.5 at pump power greater than 6 W. On the other hand, the  $\pi$  polarization maintains the beam quality factor  $M^2$  less than 1.3 over the full range of pump powers. It can be deduced that the spatial distribution of  $\sigma$ -polarized component is influenced by the presence of  $\pi$  polarization. The balance the beam quality between two polarized components is currently under further development. Figure 6 shows the measured optical spectrum for the simultaneous dual-wavelength laser at the output power intersection of the two wavelengths. The central wavelengths are 1085.7 nm ( $\sigma$  polarization) and 1088.5 nm ( $\pi$  polarization), in accord with the maximum transmission of the tilted etalon, with the spectral linewidths (FWHM) of 0.1 nm and 0.3 nm, respectively. The wavelength separation of 2.8 nm is equivalent to a frequency difference of 0.7 THz, which is significant for terahertz generation. The simultaneous dual-wavelength Nd:LuVO<sub>4</sub> laser is desirable for scientific and practical applications, especially for the development of terahertz sources. Compared with our previously published work [15], the dual-wavelength operation at 1083 nm and 1086 nm in Nd:GdVO<sub>4</sub> crystal was achieved with an almost identical experimental setup. However, both the two wavelengths were with the same polarization. Note that it is impossible to generate the dual-wavelength Nd:GdVO<sub>4</sub> laser with orthogonal polarizations in the range of 1080–1090 nm owing to the overlap between the emission distributions in  $\pi$  and  $\sigma$  polarizations.

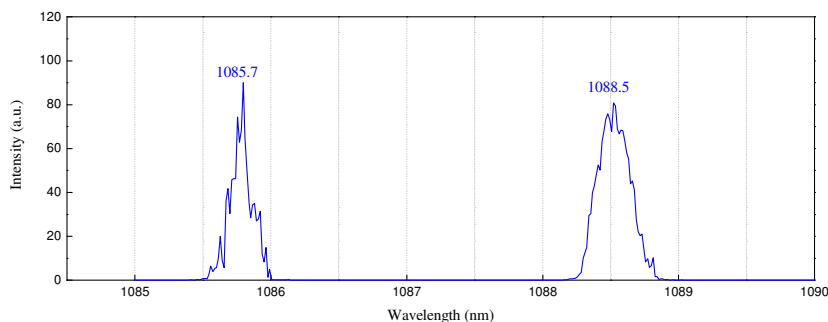


Fig. 6. Optical spectrum of dual-wavelength operation at the output power intersection.

## 5. Conclusion

The fluorescence properties of Nd:YVO<sub>4</sub>, Nd:GdVO<sub>4</sub> and Nd:LuVO<sub>4</sub> crystals for the  ${}^4F_{3/2} \rightarrow {}^4I_{11/2}$  transition have been studied and compared. It shows that the Nd-doped vanadate crystals have the comparable radiation strengths in  $\sigma$  and  $\pi$  polarizations in the range of 1080–1090 nm. In addition, Nd:LuVO<sub>4</sub> crystal specifically possesses the wider wavelength separation between the fluorescence peak positions of  $\pi$  and  $\sigma$  polarizations. Based on the superior properties of Nd:LuVO<sub>4</sub> crystal, we have numerically analyzed the condition of gain-to-loss balance via an uncoated intracavity etalon for achieving the orthogonally polarized dual-wavelength operation. A diode-pumped dual-wavelength Nd:LuVO<sub>4</sub> laser with orthogonal polarizations in the range of 1080–1090 nm has been experimentally demonstrated. The lasing wavelengths are 1085.7 nm and 1088.5 nm belonging to the  $\sigma$  and  $\pi$  polarizations, respectively. At 12 W of incident pump power, the cw output power obtained at 1085.7 nm and 1088.5 nm was 0.4 W and 1.7 W, respectively. We believed that the insertion of an etalon to control the cavity losses of two orthogonal polarizations is a simple and potential method for the low-gain line with a broad-gain bandwidth to realize the simultaneous dual-wavelength laser with orthogonal polarizations.

## Acknowledgments

The authors thank the National Science Council for the financial support of this research under Contract No. NSC-100-2628-M-009-001-MY3.